Materials Science & Engineering C 96 (2019) 51–57

Contents lists available at ScienceDirect

Materials Science & Engineering C

journal homepage: www.elsevier.com/locate/msec

Green fabrication of biologically active magnetic core-shell Fe_3O_4/Au nanoparticles and their potential anticancer effect

Zahra Izadiyan[a,*], Kamyar Shameli[a,*], Mikio Miyake[a], Sin-Yeang Teow[b], Suat-Cheng Peh[b,c], Shaza Eva Mohamad[a], Siti Husnaa Mohd Taib[a]

[a] Department of Environment and Green Technology, Malaysia-Japan International Institute of Technology, Universiti Teknologi Malaysia, Jalan Sultan Yahya Petra, 54100 Kuala Lumpur, Malaysia
[b] Department of Medical Sciences, School of Healthcare and Medical Sciences (SHMS), Sunway University, Jalan Universiti, Bandar Sunway, 47500, Selangor Darul Ehsan, Malaysia
[c] Anatomical Pathology Department, Sunway Medical Centre, Jalan Lagoon Selatan, Bandar Sunway, 47500, Selangor Darul Ehsan, Malaysia

ARTICLE INFO

Keywords:
Core-shell
Fe_3O_4/Au nanoparticles
Magnetic
Juglans regia
Green husk
Anticancer assay

ABSTRACT

Core-shell Fe_3O_4/Au nanostructures were constructed using an advanced method of two-step synthesis from *Juglans regia* (walnut) green husk extract. Several complementary methods were applied to investigate structural and magnetic properties of the samples. X-ray diffraction (XRD), high-resolution transmission electron microscopy (HR-TEM), electron diffraction, optical, thermogravimetric analysis (TGA), and vibrating sample magnetometer (VSM) were used for nanoparticle characterizations. As shown by HR-TEM, the mean diameter of core-shell Fe_3O_4/Au nanoparticles synthesized using co-precipitation method was 6.08 ± 1.06 nm. This study shows that the physical and structural properties of core-shell Fe_3O_4/Au nanoparticles possess intrinsic properties of gold and magnetite. VSM revealed that the core-shell Fe_3O_4/Au have high saturation magnetization and low coercivity due to the magnetic properties. The core-shell nanoparticles show the inhibitory concentration $(IC)_{50}$ of 235 μg/ml against a colorectal cancer cell line, HT-29. When tested against non-cancer cells, IC_{50} was not achieved even up to 500 μg/ml. This study highlights the magnetic properties and anticancer action of core-shell Fe_3O_4/Au nanoparticles. This compound can be ideal candidate for cancer treatment and other biomedical applications.

1. Introduction

The necessity of modern science and technology in novel materials with specific properties increases the interest of the global scientific community in nanophysics researchers [1,2]. In recent decades, a large number of successes and scientific data in nanotechnology allow a creation of nanomaterials with required structural, physical and chemical properties [3–5]. The ability to control structure of nanocomposite can lead to the development of new technologies in the fields of chemistry, physics and material science [6]. At present, the nanomaterials with multiple functions which can be used for various applications are of growing interest.

In recent years, inorganic nanoparticles with various compositions, physical features, and functionalities have been widely synthesized and used as drug vehicles in order to overcome multidrug-resistant cancer cells. In recent years, inorganic nanoparticles with various compositions, physical features, and functionalities have been widely synthesized and used as drug vehicles in order to overcome multidrug-resistant cancer cells [7].

In particular, core-shell nanostructures are attracting more interests due to their universal compositions and structures [8–10]. The interaction between the core and shell in a nanostructure can lead to new properties and functions [11,12]. In order to achieve different effects and physical properties, various organic and inorganic compounds can be used as materials for core and shell nanostructure constructions [13]. Materials used in core-shell nanostructures and consequently, their physical properties can make a new class of nanomaterials useful in a wide range of applications (e.g. nanomedicine, nanooptics, magnetic devices, bionanotechnology and others) [14–16].

Core-shell nanostructures can be generated by a sequential two-step synthesis, in which the core is first created and then the shell is built up [17]. In such process, the uniform coating of the core and the regulation of the shell thickness are crucial. To achieve this, the charge and selectivity of the core can be modified by polymers and surfactants,

* Corresponding author.
E-mail addresses: zahra_izadiyan@yahoo.com.my (Z. Izadiyan), kamyarshameli@gmail.com (K. Shameli).

https://doi.org/10.1016/j.msec.2018.11.008
Received 7 February 2018; Received in revised form 15 September 2018; Accepted 4 November 2018
Available online 06 November 2018
0928-4931/

thereby forming a homogeneous shell to completely cover the core [18].

There have been two types of nanomaterials: magnetic and gold nanoparticles, which have been widely exploited after the chemical synthesis of monodisperse nanoparticles is known. Magnetic nanoparticles, particularly iron and iron oxide particles such as magnetite (Fe_3O_4) and its oxidized form maghemite (γ-Fe_2O_3) with unique magnetic properties and biocompatibility have been extensively studied for a variety of biomedical applications such as hyperthermia treatment of malignant cells, magnetic resonance imaging contrast agent, magnetic separation and cell sorting, biosensors, and drug delivery [19–23]. On the other hand, gold nanoparticles have exceptional optical and chemical properties and have been shown to benefit a variety of biomedical applications such as highly sensitive diagnostics assay development, drug and gene delivery, and nucleic acids detection [24–26].

It is possible to configure magnetic nanoparticles covered with a thin layer of gold cover, this results in a core-shell nanostructure with both optical and magnetic functions in combination. Such structural assembly can additionally protect the core nanoparticles from oxidation. Moreover, the gold nanoparticles demonstrate dual functions; make binding with magnetic nanoparticles as core portion and direct contact with biological tissues. These properties make them a desired candidate in biological field and magnetic materials [27,28]. Magnetic nanoparticles hold great promise in biological and medical fields since they can be reversibly manipulated by an external magnetic field in a simple manner [29]. Meanwhile, gold nano-shell provides surface plasmon resonance in the visible range, and endows easy and straightforward linkage to biomolecules [25,30]. The amalgamation of gold with iron or iron oxide into gold-coated magnetic core-shell nanoparticles has been previously reported by various research groups [26,28,31]. Some of the common issues encountered during the core-shell nanoparticles preparation include time-consuming and laborious processes, and aggregate formation during storage.

For in vivo biological and medical applications, precise control of particle size and size distribution of nanoparticles are the key factors in determining the physicochemical and pharmacokinetic properties and subsequently their functions. However, the synthesis of uniform nanoparticles of desirable dimension still remains a great challenge. It is important to devise proper synthetic and processing strategies to obtain narrow and consistent size distribution of nanoparticles without agglomeration. In addition, a green synthesis process is preferred for future biological and medical applications.

Different parts of *Juglans regia* (*J. regia*) tree such as kernels, leaves, tree barks and fruit green husks have been utilized in both pharmaceutical and cosmetic industries [32]. A study by Carvalho et al. demonstrated the antioxidant and antimicrobial activities of walnut's leaves, seeds, and green husks [33]. *J. regia* green husk is one of the major waste products in the industry of walnut production, and little is known about its potential use in any biotechnological application. The findings from Carvalho et al. showed the potential of these low-cost natural materials to be developed into phenolic compounds for antimicrobial and antiradical applications [34]. Based on literature review, the phenolic content of *J. regia* largely varies. The high-performance liquid chromatography (HPLC) approach has been utilized and successfully identified six phenolic compounds including vanillic acid, myricetin, coumaric acid, syringic acid, juglone, and ferulic acid. Among these, juglone content was found at the highest concentration in *J. regia* green husk extraction [35].

In this work, the core-shell Fe_3O_4/Au nanostructures were obtained with a new green method by using *J. regia* as reducing agent of $HAuCl_4$ in the presence of Fe_3O_4 nanoparticles. The nanostructure is well-characterized in this study, and its potential to be developed into anticancer compound is illustrated here.

2. Experimental

2.1. Materials

Iron (III) chloride hexahydrate ($FeCl_3{\cdot}6H_2O$, 97%) and iron (II) chloride tetrahydrate ($FeCl_2{\cdot}4H_2O$, 99%) were obtained from Sigma-Aldrich (St Louis, MO, USA). Sodium hydroxide (NaOH, 99.0%) was obtained from R&M Chemicals. Gold (III) chloride trihydrate ($HAuCl_4{\cdot}3H_2O$, 99.9%) was obtained from Sigma-Aldrich, Inc., USA. The *J. regia* green husk was collected from Sorkh-e-Hesar region of Tehran, Iran. All reagents used were of analytical grades. The chemical solutions were prepared in new batches utilizing distilled water, and stored in the dark to prevent photochemical-induced reactions. All glass wares utilized in this study were cleaned with fresh HNO_3/HCl (3:1, v/v), followed by double distilled water (ddH_2O), and dried prior to use. NIH-3T3 (mouse embryonic fibroblast cell lines) and HT-29 (human colorectal adenocarcinoma cell line) as normal and cancerous cell lines were purchased from Cell Lines Service (ATCC, USA). Dulbecco's Modified Eagle's Medium (DMEM) and trypsin were obtained from Gibco (Invitrogen Corporation, UK). MTT solution was purchased from Sigma.

2.2. Synthesis of core-shell Fe_3O_4-Au nanoparticle

For the synthesis of core-shell Fe_3O_4/Au, iron oxide nanoparticles were suspended in $HAuCl_4$ solution, and the molar ratio in solution was adjusted to 1:1. The iron oxide nanoparticles suspended in the $HAuCl_4$ solution were sonicated for 20 min. *J. regia* extract was added as reducing and stabilizing agent. Finally, the Fe_3O_4/Au preparation was autoclaved for 20 min at 120 °C, the supernatant was discarded, and dried in oven dryer at 60 °C.

2.3. Structural characterization and measurements of magnetic and optical properties

The morphology, nanostructure, particle size and size distribution of the core-shell Fe_3O_4/Au nanoparticles were studied by high-resolution transmission electron microscopy (HR-TEM, JEM-2100F), while the crystal structure of the nanoparticles was analyzed by powder X-ray diffraction (XRD, Philips, X'pert, Cu Ka), the data of 2θ being typically collected in the range of 10–90°. To run the elemental analysis of the Au-NPs, energy dispersion X-ray spectroscopy was carried out on a Shimadzu EDX700HS spectrometer attached to the FESEM. The magnetic property was measured on a Lakeshore vibrating sample magnetometer (VSM) on the dried samples at room temperature and the sample was measured in powder form. Furthermore, the optical properties of the samples were characterized by a UV–vis spectrometer (UV–vis 1800, SHIMADZU), revealing the surface plasmon resonance characteristic of the nanostructured Au surface. The amount of gold coating the iron oxide nanoparticles was determined by thermogravimetric analysis (TGA) using a TGA Q50 V20 with a 10 °C/min heating rate under a nitrogen atmosphere (10 ml min^{-1}). The measurement was made from 10 °C up to 800 °C.

2.4. Cytotoxicity assay

Cytotoxicity assay measures the killing capacity of test compound against a target cell. One of the common methods to determine cytotoxicity is by MTT (3-[4,5-dimethylthiazol-2-yl]-2,5-diphenyltetrazolium bromide) assay. Mouse embryonic fibroblast cell lines (NIH-3T3) and human colorectal adenocarcinoma cell line (HT-29) as normal and cancerous cell lines were used in this study. Cultured cells at concentration of 2000 cells/well was prepared and plated (100 µl/well) onto 96-well plates. The diluted sample extracts were added to each well with known concentrations; 1, 20, 62.5, 125, 250, and 500, µg/ml. The cells were then incubated for 72 h at 37 °C in a 5% CO_2 incubator.

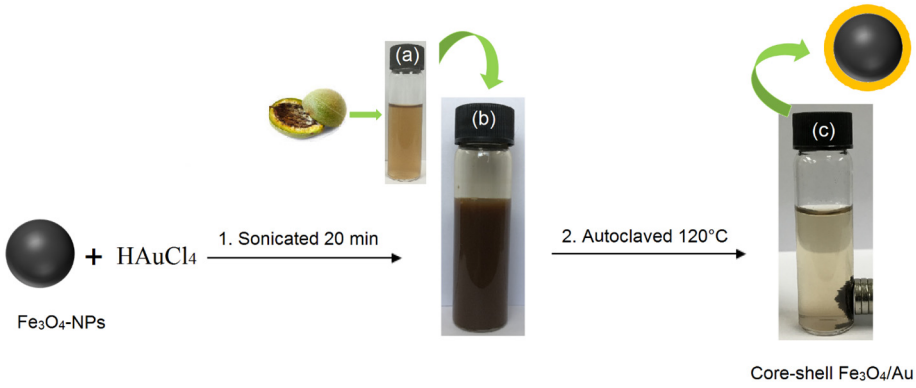

Fig. 1. (a) *J. regia* extract. (b) Fe_3O_4-NPs and $HAuCl_4$ solution. (c) Separation of synthesized core shell Fe_3O_4-NPs from reaction mixture using an external magnet. (For interpretation of the references to color in this figure, the reader is referred to the web version of this article.)

MTT solution was then added to each well and incubated for additional 3 h at 37 °C in the 5% CO_2 incubator. After solubilization of the purple formazan crystals using dimethyl sulfoxide (DMSO), the optical density (OD) of the well was measured using an ELISA reader (Tecan, Sunrise) at a wavelength of 570 nm. The cytotoxicity was recorded as the drug concentration causing 50% growth inhibition of the tumor cells (IC_{50} value) using the formula given below in the Eq. (1) and an inhibition graph was plotted. The images of HT-29 and NIH-3T3 before and after treatment were also assessed by inverted microscope attached to a camera system (Nikon, Eclipse, TS100, ElWD 0.3/OD75).

$$\%\text{Cell viability} = \frac{\text{OD test sample (mean)}}{\text{OD control (mean)}} \times 100 \quad (1)$$

3. Results and discussion

The mixture of Fe_3O_4-NPs and $HAuCl_4$ solution was sonicated for 20 min and the color of the reaction mixture turned to dark brown. The *J. regia* extract (Fig. 1a) was added to the mixture (Fig. 1b) and autoclaved for 20 min at 120 °C. The color changed from dark brown (Fig. 1b) to very dark purple (Fig. 1c), which indicate the formation of core shell Fe_3O_4-NPs. The separation of core shell Fe_3O_4-NPs could be accomplished with the aid of an external magnet. Fig. 1c clearly reveals that the synthesized cFe_3O_4-NPs is able to be attracted by an external magnet, which proved that the nanoparticles possessed magnetic properties. After the magnet was removed, the nanoparticles could be dispersed readily by shaking.

4. Characterization of the Fe_3O_4/Au by XRD and HR-TEM

Fig. 2 illustrates XRD patterns of Fe_3O_4 and core-shell Fe_3O_4/Au nanoparticles. Magnetite nanoparticles have cubic structure. According to the standard database, this corresponds to the phase of Fe_3O_4 (Ref. No. 01-075-0449). The reflections are significantly broadened, indicating small size of the particles. The particle size estimated from the broadening of the (311) reflex by the Scherrer formula was found to be about 1.89 nm. X-ray analysis of the core-shell Fe_3O_4/Au (Fig. 2) revealed the presence of single gold phase with a face-centered cubic lattice. The average size of coherent scattering regions was about 3.44 nm. The weak contribution from iron oxide Fe_3O_4 to the X-ray diffraction pattern of Fe_3O_4/Au can be explained by shielding the core by heavy Au atoms at the particle surface. In the thinner, Au-shell sample demonstrates four weak peaks (200), (311), (511) and (440) of Fe_3O_4, in addition to the normal gold peaks. It implies that X-ray can penetrate to the core of Fe/Fe_3O_4 if the gold shell is not sufficiently thick; otherwise, the signal from the core is shielded to become visible in the XRD pattern. The absence of any diffraction peaks for magnetite is most likely due to the heavy atom effect from gold as a result of the

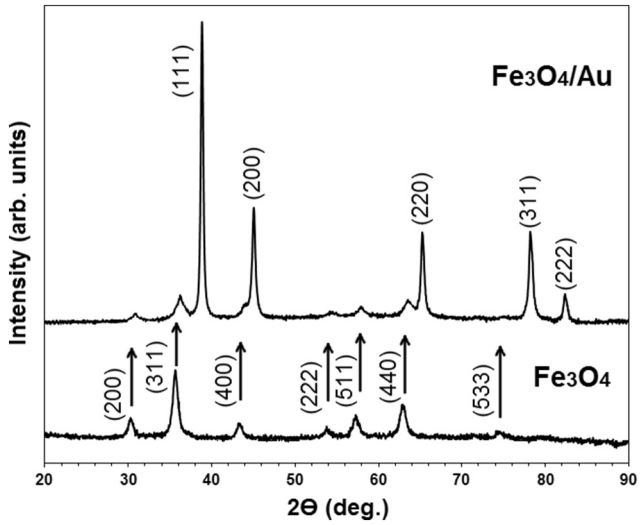

Fig. 2. X-ray diffraction patterns of Fe_3O_4 and core-shell Fe_3O_4/Au nanoparticles.

formation of Au-coated Fe_3O_4 nanocrystals [26]. Thus, our results indicate that X-rays can penetrate into the core when the Au shell is thin enough; otherwise, the XRD signal from the nucleus is screened by gold and becomes invisible. This shows that the ability of XRD method to identify the core structure in Fe_3O_4/Au nanoparticles depends on the thickness of the gold shell.

Fig. 3 shows the HR-TEM image and histogram of Fe_3O_4/Au showing particle size distribution. Our previous study showed that the Fe_3O_4 nanoparticles have cubic with size of about 5.77 nm, which is consistent with this XRD data [36]. Dark color Particles in dark color are shown in Fig. 3 corresponding to the Fe_3O_4 covered by gold at an intermediate stage of synthesis. As seen in HR-TEM image, Fe_3O_4/Au nanoparticles have increased size with a diameter of about 6.08 nm after gold coating. Dark and light areas in Fig. 3 represent the Fe_3O_4 and Au, respectively. Single-crystalline state can be seen in Fig. 4 with typical atomic layers of gold and magnetite. As shown in insets of Fig. 4 the calculated inter-atomic spacing of 0.259 and 0.229 nm correspond to the (311) plane of magnetite and (111) plane of gold, respectively.

Fig. 5 depicts the distribution size and identification of the core-shell Fe_3O_4/Au nanoparticles using FESEM image and EDX. The structure of core-shell Fe_3O_4/Au nanoparticles showed a mass with a specific form, which was the typical shape of Au. Fig. 5a represents the synthesis of core-shell Fe_3O_4/Au nanoparticles with $HAuCl_4$ solution on coted on the surface of Fe_3O_4.

As shown in Fig. 5b of the EDXRF patterns for the core-shell Fe_3O_4/Au nanoparticles confirmed the presence of Au and Fe in the core-shell

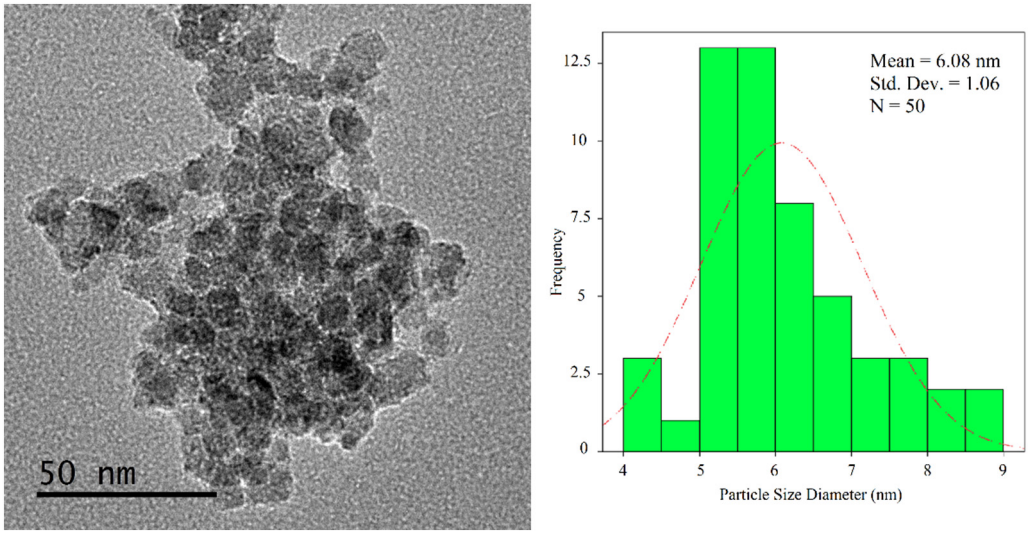

Fig. 3. HR-TEM images of Fe_3O_4/Au nanoparticles and particle size distribution of Fe_3O_4/Au.

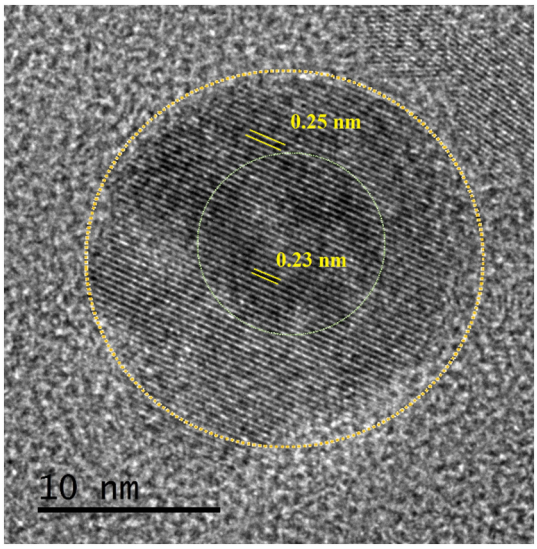

Fig. 4. HR-TEM image of Fe_3O_4/Au nanoparticles. Insets show the calculated inter-atomic distances of the (111) plane in gold and the (311) plane in magnetite. (For interpretation of the references to color in this figure legend, the reader is referred to the web version of this article.)

Fe_3O_4/Au nanoparticles without any impurity peaks in Fig. 5b. Each element has a unique atomic structure, EDXRF provides information about the chemical composition of the compound. EDXRF is an interaction between X-rays and the compound being investigated. Therefore, when this analysis is carried out, the X-rays that are reflected off the compound give peaks. The amplitude of the peaks obtained help to identify the elements present in the compound being studied. A strong Au and Fe peaks in the figure showed that core-shell Fe_3O_4/Au nanoparticles were successfully fabricated. The EDXRF spectra revealed the presence of gold peaks in four different areas and iron peaks in two different areas (Fig. 5b). The EDXRF spectra clearly showed the percentage yields for Fe_3O_4 and Au were 29.89% and 43.83%, respectively. The results indicated that the biosynthesized nanoparticles were composed of high purity core-shell Fe_3O_4/Au nanoparticles.

4.1. UV–visible spectroscopy analysis

Fig. 6 shows the optical absorption spectra of the individual Au, Fe_3O_4 nanoparticles and core-shell Fe_3O_4/Au nanoparticles dispersed in water. The obtained data demonstrate an absence of plasmon lines in the Fe_3O_4 nanoparticles (Fig. 6b), while the gold nanoparticles show a band of plasmon resonance with a maximum at the wavelength of 537 nm (Fig. 6a).

In nanoparticles Fe_3O_4/Au, a detected peak is broadened and shifted to a red region with respect to the signal from gold nanoparticles at the wavelength of 554 nm (Fig. 6c). A red shift is related to the dielectric

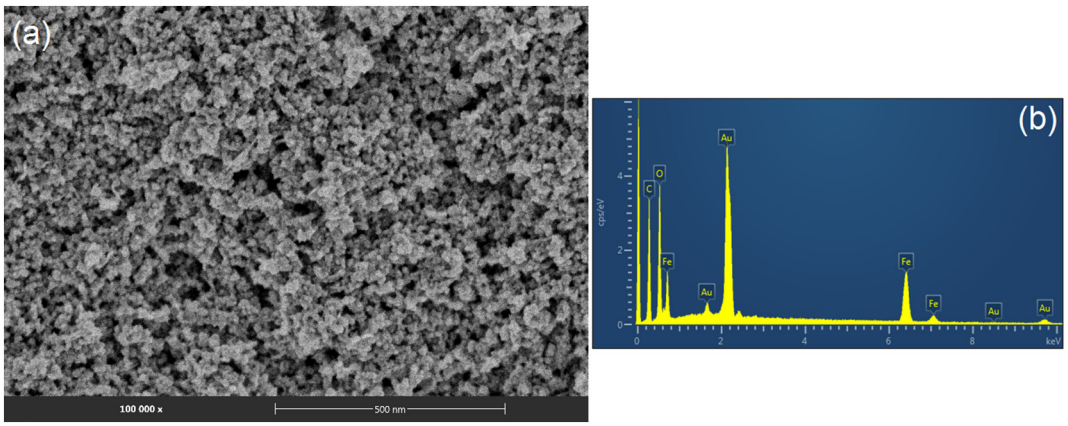

Fig. 5. (a) FESEM micrographs and (b) EDXRF spectra for the core-shell Fe_3O_4/Au nanoparticles.

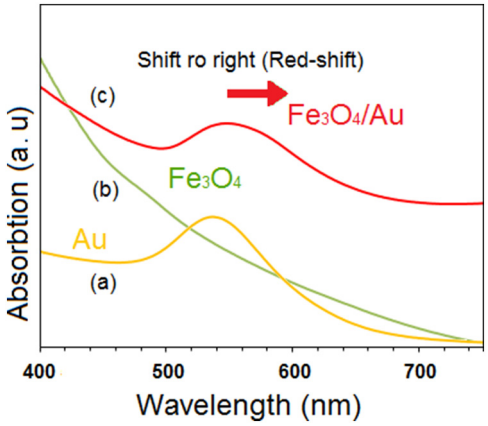

Fig. 6. Absorption spectra of Au (a), Fe_3O_4 (b), and Fe_3O_4/Au (c) samples.

constant, which is inversely proportional to plasmon oscillation frequency. Quantum-size effects in modified nanostructures can give the rise to a red shift of this frequency due to the change in a dielectric constant [37]. The peak broadening is associated with isolation of the Fe_3O_4/Au nanoclusters dispersed in water, which decreases the electronic exchange between gold nanoparticles [37].

4.2. Vibrating sample magnetometer

Fig. 7 shows the hysteresis curves of the Fe_3O_4 and Fe_3O_4/Au composite, separately recorded by VSM. It can be seen from the magnetization curves that high saturation magnetization (Ms) of the *J. regia*/iron oxide nanoparticles (53.32 emu·g^{-1}) and core-shell (45.06 emu·g^{-1}) with low coercivity 32.50 Oe and 12.05 Oe were obtained, respectively. The results show that the Fe_3O_4 nanocrystals are near soft ferromagnetic, while the *J. regia*-processed Fe_3O_4/Au nanoparticles are near superparamagnetic with a small coercivity at room temperature. Significantly, the comparison of the curves indicates that the core-shell Fe_3O_4/Au nanoparticles processed with either *J. regia* are much easier to saturate than the Fe_3O_4 nanoparticles with larger particle sizes. The corresponding magnetization decreases rapidly with respect to the core-shell nanoparticles and therefore the susceptibility becomes smaller. As a result, the *J. regia*-processed core-shell Fe_3O_4/Au nanoparticles with lower susceptibility can still increase the performance of the operation and offer potential applications in various areas.

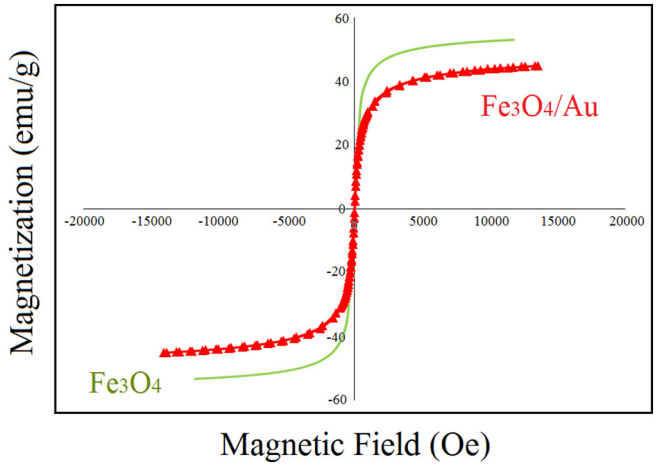

Fig. 7. Vibrating sample magnetometer plots of Fe_3O_4 and Fe_3O_4 coated with Au nanoparticles.

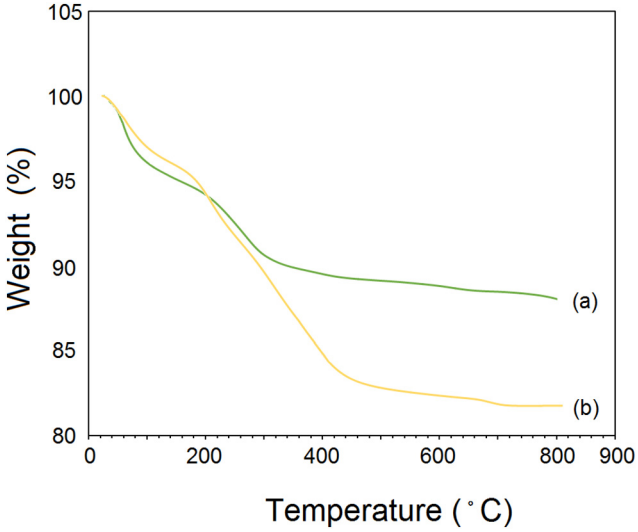

Fig. 8. Weight loss of magnetic particles coated with Au, the thermogram of *J. regia*/iron oxide nanoparticles (a) and core-shell Fe_3O_4/Au (b) has been included.

4.3. Thermogravimetric analysis

Both TGA curves show a slight loss of weight in the temperature range of 30–100 °C due to the moisture content in the sample. As shown in Fig. 8a and b, the mass profile exhibited a well-defined decrease over a temperature range of 100–340 °C. This weight loss was due to desorption and subsequent evaporation of *J. regia*. Based on the Fig. 8a from 340 to 800 °C transformation of Fe_3O_4 to γ Fe_2O_3 and Fe_2O_3 to α Fe_2O_3 were obtained [38]. In Fig. 8b, the weight loss from 177 to 425 °C was due to the gold content in the sample, while from 440 to 800 °C, the transformation of Fe_3O_4 to γ-Fe_2O_3 and Fe_2O_3 to α-Fe_2O_3 were obtained. According to the result the final weight loss of *J. regia*/iron oxide nanoparticle and core-shell Fe_3O_4/Au are 88.03% and 81.87%, respectively, then, 6.16% of weight loss is due to evaporation of Au shell.

4.4. In vitro cytotoxicity and anticancer assays

As shown in Fig. 9, the cytotoxicity effects of the synthesized core-shell Fe_3O_4/Au were investigated on NIH-3T3 (mouse embryonic fibroblast cell lines) and HT-29 [39–41] (human colorectal adenocarcinoma cell line) as normal and cancerous cell lines, respectively. The cells were treated with the core-shell Fe_3O_4/Au at various concentrations (1–500 μg/ml) and incubated at 37 °C, 5% CO_2 for 72 h. IC_{50} could not be determined for normal cell line even up to 500 μg/ml. On the other hand, the nanoparticles exhibited toxic effect on cancerous cell line, HT-29 (IC_{50} estimated to be 235 μg/ml) (Fig. 9a). The Fe_3O_4/Au nanoparticles demonstrated no significant toxicity on normal cell line, suggesting that the core-shell Fe_3O_4/Au nanoparticles are well-tolerated by NIH-3T3 cells (Fig. 9b). These results highlight the potential of developing these nanoparticles into anticancer compound. In a previous study, the bio-functional starch/iron oxide nanoparticles have non-toxic effects on normal and cancerous cervical cell lines which is in line with current study, making them suitable candidates for various biological and medical applications [42].

Fig. 10(a and c) shows images of cell lines in the absence of core-shell Fe_3O_4/Au. The images show the typical morphology of fibroblasts and epithelial cells. Fig. 10d represents the image of cells in the presence of core-shell Fe_3O_4/Au. The nanoparticles interacted with treated cells and resulted in a significant cell death. In the treated-NIH3T3, the cells retained the typical morphology of fibroblasts in vital state.

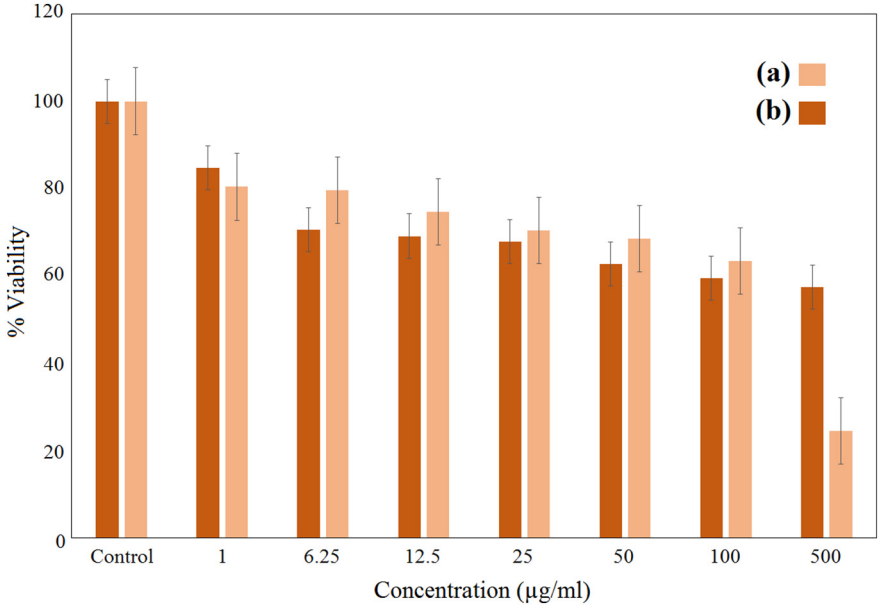

Fig. 9. MTT assays in (a) line human colorectal adenocarcinoma (HT-29) cell line and (b) mouse fibroblast (NIH-3T3) cell after 72 h of treatment with core-shell Fe_3O_4/Au.

5. Conclusion

An advanced method was used to synthesize core-shell Fe_3O_4/Au nanoparticles from *J. regia* green husk. The formation of the core-shell Fe_3O_4/Au structure was carried out by seeding the Fe_3O_4 core followed by the coating of the gold nano-shell. The XRD patterns show the crystal structure of the core-shell, while TEM provides the knowledge of morphology, mono-crystallinity, nanostructure, particle size, and distribution. The magnetic properties of the nanoparticles were characterized by VSM, which shows excellent susceptibility, and the UV–vis spectrum reveals the well-defined surface plasmon at the 554 nm characteristic of the core-shell Fe_3O_4/Au, substantiating the formation of a tight Au-shell on the Fe_3O_4 surface. The materials obtained have the prospects for development and application, in particular, for biomedical targeted drug delivery. As shown in our study, magnetic properties, which are slightly decreased by the coating of nanoparticles with gold, further contribute to their promising applications due to the nontoxicity and biocompatibility providing by a noble metal in the nanoparticle shell. This concept is planned in our following experiments to be explored.

Acknowledgments

The researcher would like to express sincere gratitude to the university technology malaysia under research university grant Tier 1 [grant number Q.K.130000.2543.20H55, Q.K.130000.2543.20H33, Q.K.130000.2543.17H60]. All authors also would like to thank the Malaysia Japan International Institute of Technology (MJIIT) of UTM

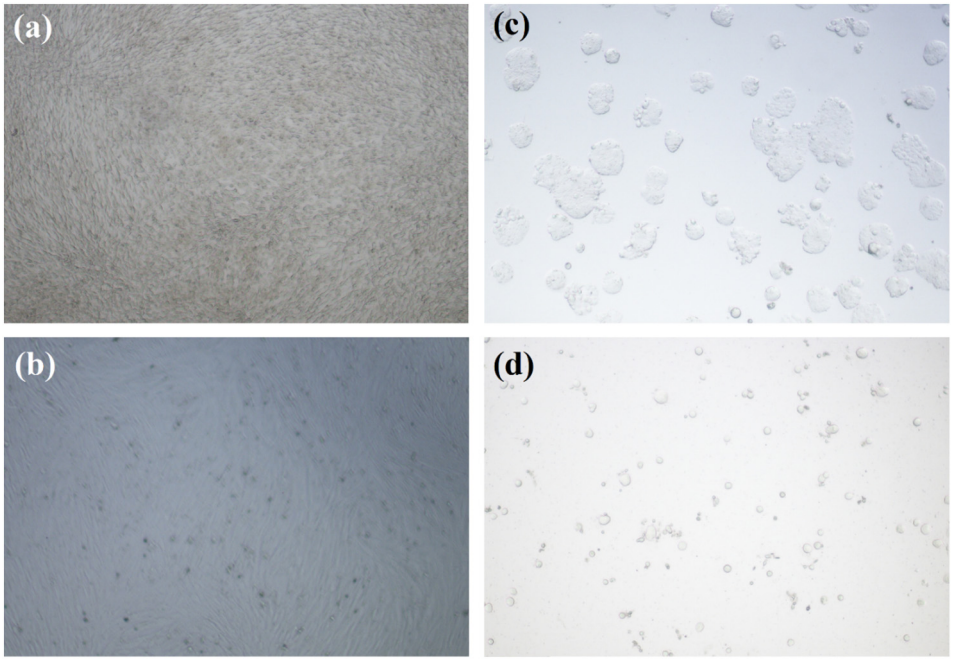

Fig. 10. Microscopic images of core-shell Fe_3O_4/Au on NIH-3T3 [control and treated cell (a–b)] and HT-29 [control and treated cell (c–d)].

for the conducive research environment.

References

[1] A. Baskakov, A.Y. Solov'eva, Y.V. Ioni, S. Starchikov, I. Lyubutin, I. Khodos, A. Avilov, S. Gubin, Magnetic and interface properties of the core-shell Fe_3O_4/Au nanocomposites, Appl. Surf. Sci. 422 (2017) 638–644.

[2] D. Bhattacharyya, S. Singh, N. Satnalika, A. Khandelwal, S.-H. Jeon, Nanotechnology, big things from a tiny world: a review, Nanotechnology 2 (2009) 29–38.

[3] T.-C. Chang, F.-Y. Jian, S.-C. Chen, Y.-T. Tsai, Developments in nanocrystal memory, Mater. Today 14 (2011) 608–615.

[4] S. Chaturvedi, P.N. Dave, Emerging applications of nanoscience, Materials Science Forum, Trans Tech Publ, 2014, pp. 25–32.

[5] D.L. Schodek, P. Ferreira, M.F. Ashby, Nanomaterials, Nanotechnologies and Design: An Introduction for Engineers and Architects, Butterworth-Heinemann, 2009.

[6] B. Bhushan, Nanotribology and nanomechanics, Wear 259 (2005) 1507–1531.

[7] H.-Y. Lian, M. Hu, C.-H. Liu, Y. Yamauchi, K.C.-W. Wu, Highly biocompatible, hollow coordination polymer nanoparticles as cisplatin carriers for efficient intracellular drug delivery, Chem. Commun. 48 (2012) 5151–5153.

[8] M.B. Gawande, A. Goswami, T. Asefa, H. Guo, A.V. Biradar, D.-L. Peng, R. Zboril, R.S. Varma, Core–shell nanoparticles: synthesis and applications in catalysis and electrocatalysis, Chem. Soc. Rev. 44 (2015) 7540–7590.

[9] A. Bachhuka, S.N. Christo, A. Cavallaro, K.R. Diener, A. Mierczynska, L.E. Smith, R. Marian, J. Manavis, J.D. Hayball, K. Vasilev, Hybrid core/shell microparticles and their use for understanding biological processes, J. Colloid Interface Sci. 457 (2015) 9–17.

[10] R.G. Chaudhuri, S. Paria, Core/shell nanoparticles: classes, properties, synthesis mechanisms, characterization, and applications, Chem. Rev. 112 (2012) 2373–2433.

[11] Z. Wang, H. Fu, Z. Tian, D. Han, F. Gu, Strong metal–support interaction in novel core–shell Au–CeO_2 nanostructures induced by different pretreatment atmospheres and its influence on CO oxidation, Nanoscale 8 (2016) 5865–5872.

[12] X. Wang, Y. Cui, S. Yu, Q. Zeng, M. Yang, Core–shell interaction and its impact on the optical absorption of pure and doped core-shell CdSe/ZnSe nanoclusters, J. Chem. Phys. 144 (2016) 134307.

[13] Y.S. Kim, S.M. Lee, P. Govindaiah, S.J. Lee, S.H. Lee, J.H. Kim, I.W. Cheong, Multifunctional Fe_3O_4 nanoparticles-embedded poly (styrene)/poly (thiophene) core/shell composite particles, Synth. Met. 175 (2013) 56–61.

[14] D. Knopp, D. Tang, R. Niessner, Bioanalytical applications of biomolecule-functionalized nanometer-sized doped silica particles, Anal. Chim. Acta 647 (2009) 14–30.

[15] T. Mitsudome, K. Kaneda, Advanced core–shell nanoparticle catalysts for efficient organic transformations, ChemCatChem 5 (2013) 1681–1691.

[16] V. Pustovalov, L. Astafyeva, W. Fritzsche, Optical properties of core–shell gold--silver and silver–gold nanoparticles for near UV and visible radiation wavelengths, Plasmonics 7 (2012) 469–474.

[17] A.M. El-Toni, M.A. Habila, J.P. Labis, Z.A. ALOthman, M. Alhoshan, A.A. Elzatahry, F. Zhang, Design, synthesis and applications of core–shell, hollow core, and nanorattle multifunctional nanostructures, Nanoscale 8 (2016) 2510–2531.

[18] Y. Cao, B. Wang, Y. Wang, D. Lou, Polymer-controlled core–shell nanoparticles: a novel strategy for sequential drug release, RSC Adv. 4 (2014) 30430–30439.

[19] L. Josephson, J.M. Perez, R. Weissleder, Magnetic nanosensors for the detection of oligonucleotide sequences, Angew. Chem. 113 (2001) 3304–3306.

[20] H. Pardoe, W. Chua-Anusorn, T.G.S. Pierre, J. Dobson, Structural and magnetic properties of nanoscale iron oxide particles synthesized in the presence of dextran or polyvinyl alcohol, J. Magn. Magn. Mater. 225 (2001) 41–46.

[21] W. Wu, Q. He, C. Jiang, Magnetic iron oxide nanoparticles: synthesis and surface functionalization strategies, Nanoscale Res. Lett. 3 (2008) 397.

[22] S.R. Dave, X. Gao, Monodisperse magnetic nanoparticles for biodetection, imaging, and drug delivery: a versatile and evolving technology, Wiley Interdisciplinary Reviews: Nanomedicine and Nanobiotechnology, 1 2009, pp. 583–609.

[23] H.-Y. Lee, S.-H. Lee, C. Xu, J. Xie, J.-H. Lee, B. Wu, A.L. Koh, X. Wang, R. Sinclair, S.X. Wang, Synthesis and characterization of PVP-coated large core iron oxide nanoparticles as an MRI contrast agent, Nanotechnology 19 (2008) 165101.

[24] Z. Izadiyan, K. Shameli, H. Hara, S.H.M. Taib, Cytotoxicity assay of biosynthesis gold nanoparticles mediated by walnut (*Juglans regia*) green husk extract, J. Mol. Struct. 1151 (2017) 97–105.

[25] M.-C. Daniel, D. Astruc, Gold nanoparticles: assembly, supramolecular chemistry, quantum-size-related properties, and applications toward biology, catalysis, and nanotechnology, Chem. Rev. 104 (2004) 293–346.

[26] H. Liu, P. Hou, W. Zhang, J. Wu, Synthesis of monosized core–shell Fe_3O_4/Au multifunctional nanoparticles by PVP-assisted nanoemulsion process, Colloids Surf. A Physicochem. Eng. Asp. 356 (2010) 21–27.

[27] B.I. Kharisov, O.V. Kharissova, M.J. Yacaman, State of the art of the bi-and trimetallic nanoparticles on the basis of gold and iron, Recent Pat. Nanotechnol. 3 (2009) 81–98.

[28] H.-L. Liu, J.-H. Wu, J.H. Min, J.H. Lee, Y.K. Kim, Monosized core–shell Fe_3O_4 (Fe)/Au multifunctional nanocrystals, J. Nanosci. Nanotechnol. 9 (2009) 754–758.

[29] D.L. Huber, Synthesis, properties, and applications of iron nanoparticles, Small 1 (2005) 482–501.

[30] I.H. El-Sayed, X. Huang, M.A. El-Sayed, Surface plasmon resonance scattering and absorption of anti-EGFR antibody conjugated gold nanoparticles in cancer diagnostics: applications in oral cancer, Nano Lett. 5 (2005) 829–834.

[31] L. Wang, L. Wang, J. Luo, Q. Fan, M. Suzuki, I.S. Suzuki, M.H. Engelhard, Y. Lin, N. Kim, J.Q. Wang, Monodispersed core–shell Fe_3O_4@ Au nanoparticles, J. Phys. Chem. B 109 (2005) 21593–21601.

[32] F. Stampar, A. Solar, M. Hudina, R. Veberic, M. Colaric, Traditional walnut liqueur–cocktail of phenolics, Food Chem. 95 (2006) 627–631.

[33] A. Fernández-Agulló, E. Pereira, M. Freire, P. Valentao, P. Andrade, J. González-Álvarez, J. Pereira, Influence of solvent on the antioxidant and antimicrobial properties of walnut (*Juglans regia* L.) green husk extracts, Ind. Crop. Prod. 42 (2013) 126–132.

[34] M. Carvalho, P.J. Ferreira, V.S. Mendes, R. Silva, J.A. Pereira, C. Jerónimo, B.M. Silva, Human cancer cell antiproliferative and antioxidant activities of *Juglans regia* L, Food Chem. Toxicol. 48 (2010) 441–447.

[35] S.N. Cosmulescu, I. Trandafir, G. Achim, B. Mihai, A. Baciu, M. Gruia, Phenolics of green husk in mature walnut fruits, Not. Bot. Horti Agrobo. Cluj-Napoca 38 (2010) 53.

[36] Z. Izadiyan, K. Shameli, M. Miyake, H. Hara, S.E.B. Mohamad, K. Kalantari, S.H.M. Taib, E. Rasouli, Cytotoxicity assay of plant-mediated synthesized iron oxide nanoparticles using *Juglans regia* green husk extract, Arab. J. Chem. (2018) (In Press).

[37] R.T. Tom, A.S. Nair, N. Singh, M. Aslam, C. Nagendra, R. Philip, K. Vijayamohanan, T. Pradeep, Freely dispersible Au@ TiO_2, Au@ ZrO_2, Ag@ TiO_2, and Ag@ ZrO_2 core–shell nanoparticles: one-step synthesis, characterization, spectroscopy, and optical limiting properties, Langmuir 19 (2003) 3439–3445.

[38] S. García-Jimeno, J. Estelrich, Ferrofluid based on polyethylene glycol-coated iron oxide nanoparticles: characterization and properties, Colloids Surf. A Physicochem. Eng. Asp. 420 (2013) 74–81.

[39] Y. Yang, J. Aw, K. Chen, F. Liu, P. Padmanabhan, Y. Hou, Z. Cheng, B. Xing, Enzyme-responsive multifunctional magnetic nanoparticles for tumor intracellular drug delivery and imaging, Chem. Asian J. 6 (2011) 1381–1389.

[40] S. Eynali, S. Khoei, S. Khoee, E. Esmaelbeygi, Evaluation of the cytotoxic effects of hyperthermia and 5-fluorouracil-loaded magnetic nanoparticles on human colon cancer cell line HT-29, Int. J. Hyperth. 33 (2017) 327–335.

[41] S. Jung, X. Chen, Natural killer cell labeled by gold-coated iron oxide nanoparticles: PET/MRI/PA monitoring and immuno-photothermal cancer therapy, J. Nucl. Med. 59 (2018) 194.

[42] A. Gholoobi, Z. Meshkat, K. Abnous, M. Ghayour-Mobarhan, M. Ramezani, F.H. Shandiz, K. Verma, M. Darroudi, Biopolymer-mediated synthesis of Fe_3O_4 nanoparticles and investigation of their in vitro cytotoxicity effects, J. Mol. Struct. 1141 (2017) 594–599.